Journal of the Physical Society of Japan
Vol. 77, No. 10, October, 2008, 103710

Evolution of an Unconventional Superconducting State inside the Antiferromagnetic Phase of $CeNiGe_3$ under Pressure: A ^{73}Ge-Nuclear-Quadrupole-Resonance Study

Atsushi HARADA*, Hidekazu MUKUDA, Yoshio KITAOKA, Arumugam THAMIZHAVEL[1], Yusuke OKUDA[1], Rikio SETTAI[1], Yoshichika ŌNUKI[1], Kouhei M. ITOH[2], Eugene E. HALLER[3], and Hisatomo HARIMA[4]

Department of Materials Engineering Science, Osaka University, Toyonaka, Osaka 560-8531
[1]*Department of Physics, Osaka University, Toyonaka, Osaka 560-0043*
[2]*Department of Applied Physics and Physico-Informatics, Keio University, Yokohama 223-8522*
[3]*Department of Materials Science and Engineering, University of California at Berkeley and Lawrence Berkeley National Laboratory, Berkeley, CA 94720, U.S.A.*
[4]*Department of Physics, Faculty of Science, Kobe University, Kobe 657-8501*

(Received July 22, 2008; accepted August 29, 2008; published October 10, 2008)

We report a ^{73}Ge nuclear-quadrupole-resonance (NQR) study on novel evolution of unconventional superconductivity in antiferromagnetic (AFM) $CeNiGe_3$. The measurements of the ^{73}Ge-NQR spectrum and the nuclear spin–lattice relaxation rate ($1/T_1$) have revealed that the unconventional superconductivity evolves inside a commensurate AFM phase around the pressure (P) where Néel temperature T_N exhibits its maximum at 8.5 K. The superconducting transition temperature T_{SC} has been found to be enhanced with increasing T_N, before reaching the quantum critical point at which the AFM order collapses. Above T_{SC}, the AFM structure transits from an incommensurate spin-density-wave order to a commensurate AFM order at $T \sim 2$ K, accompanied by a longitudinal spin-density fluctuation. With regard to heavy-fermion compounds, these novel phenomena have hitherto never been reported in the P–T phase diagram.

KEYWORDS: heavy fermion, superconductivity, $CeNiGe_3$, commensurate and incommensurate antiferromagnetism, NQR under pressure
DOI: 10.1143/JPSJ.77.103710

Since the discovery of the heavy-fermion (HF) superconductor $CeCu_2Si_2$,[1] the interplay between superconductivity and magnetism has been one of the most attractive subjects in condensed matter physics. The HF superconductivity often appears near a quantum critical point (QCP) where antiferromagnetism is suppressed by an application of pressure (P) in cerium(Ce)-based compounds such as $CeCu_2Ge_2$,[2] $CePd_2Si_2$,[3] $CeRh_2Si_2$,[4] $CeIn_3$,[5] and $CeRhIn_5$.[6] Because of strong antiferromagnetic (AFM) correlation near the QCP, the above finding suggests that the mechanism forming Cooper pairs can be magnetic in origin. Namely, near the QCP, the magnetically soft electron liquid can mediate spin-dependent attractive interactions between the charge carriers. In addition to the emergence of P-induced superconductivity above the QCP, another interesting phenomenon is the coexistence of superconductivity and antiferromagnetism below the QCP.[7–9]

The HF antiferromagnet $CeNiGe_3$ ($T_N = 5.5$ K) has been reported to become superconducting (SC) under P.[10] The most remarkable feature is that P-induced superconductivity emerges in two P ranges of 1.7–3.7 GPa and 5.9–7.3 GPa, where zeroresistivity is observed.[11] Here, we denote the two SC domes in a low and high P region as SC1 and SC2, respectively, as shown in Fig. 1. In this figure, an application of P makes T_N increase and exhibit its maximum at 8.5 K around $P \sim 3$ GPa, and disappears around $P \sim 7$ GPa.[11,12] Interestingly, SC1 seems to appear inside the AFM phase, exhibiting a maximum of $T_{SC} \sim 0.3$ K at the maximum value of T_N, whereas SC2 emerges around the QCP where the AFM order collapses, as reported thus far.[11] The emergence of SC1 may be due to the delocalization of Ce 4f electrons, even though the AFM order is robust against the application of P, which causes T_N and the internal magnetic field to increase.[12] These experimental results suggest that the emergence of SC1 relates to a novel type of SC mechanism, which differs from that in SC2 near the QCP.

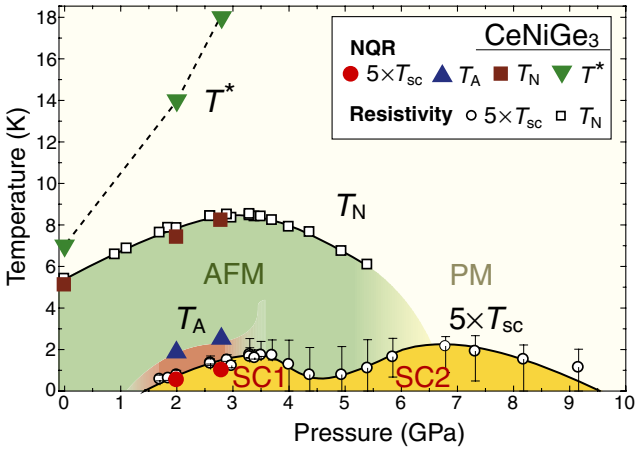

Fig. 1. (Color online) Pressure vs temperature phase diagram of $CeNiGe_3$ established by resistivity[11] along with the results of this study. The error bars represent the width of the SC transition between its onset and zeroresistivity, respectively.[11] T^* is a crossover temperature from the localized to the itinerant regimes for the 4f electrons. We revealed a transition of the AFM structure, denoted as T_A at $P = 2.0$ and 2.8 GPa where SC1 takes place (see text).

*E-mail: HARADA.Atsushi@nims.go.jp

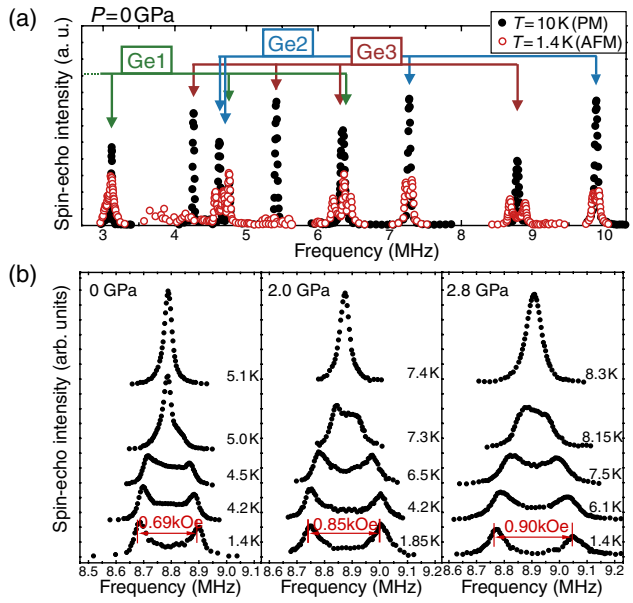

Fig. 2. (Color online) (a) ^{73}Ge-NQR spectra for the PM state at $T = 10$ K (solid circles) and for the AFM state at 1.4 K (open circles) at $P = 0$ GPa. (b) Temperature dependence of the $4\nu_Q$ transition for the Ge3 site ($f \sim 8.8$ MHz) at $P = 0$, 2.0, and 2.8 GPa. The spectra for the PM state are shown at the top of each figure, while the others for the AFM state at each P.

In this letter, we report on the novel characteristics of antiferromagnetism and SC1 observed from the ^{73}Ge-NQR measurements under P at zero field ($H = 0$). We reveal that an unconventional SC1 emerges under the background of a commensurate AFM structure in which an incommensurate spin-density-wave order changes around $T \sim 2$ K well below T_N. It is demonstrated that the P-induced SC1 in $CeNiGe_3$ occurs in such a characteristic AFM state that the application of P increases T_N inside the AFM phase far from the QCP.

A polycrystalline sample enriched with ^{73}Ge was crushed into a powder in order to allow RF pulses to penetrate into the samples easily for NQR measurements. The NQR measurements were performed by the conventional spin–echo method in a frequency (f) range of 2.8–10 MHz at $P = 0$, 2.0, and 2.8 GPa. A ^{3}He-^{4}He dilution refrigerator was used to obtain the lowest temperature (T) of 50 mK. A BeCu/NiCrAl piston-cylinder P cell with a P-transmitting medium of poly(ethylsiloxane) (PES-1) was used to generate hydrostatic P.[13] The value of P was determined from the T_{SC} of Sn obtained from the resistivity measurements.

Figure 2(a) indicates the well-articulated spectra of ^{73}Ge-NQR for a nuclear spin $I = 9/2$ which arises from three Ge sites. By incorporating the NQR parameters (ν_Q, η) obtained from the band calculation by Harima *et al.*, each NQR peak is considered to arise from the Ge1 ($V_{zz} \parallel b$), Ge2 ($V_{zz} \parallel c$), and Ge3 ($V_{zz} \parallel b$) sites in $CeNiGe_3$ as shown in the figure where the simulated spectra are presented and each NQR frequency is indicated by an arrow.[12] It should be noted that all these spectra are affected by the emergence of the internal field H_{int} at each Ge site below T_N, confirming absence of a paramagnetic (PM) phase at $P = 0$, 2.0, and 2.8 GPa. T_1 and T_2 were measured at the $4\nu_Q$ ($\pm 7/2 \leftrightarrow \pm 9/2$) transition of the Ge1 site ($f \sim 6.3$ MHz) because this transition is well resolved from the others below T_N. On the other hand, in the PM at $P = 0$, they were measured at the $2\nu_Q$ ($\pm 3/2 \leftrightarrow \pm 5/2$) transition of the Ge1 site ($f \sim 3.1$ MHz) because the $4\nu_Q$ of the Ge1 site accidentally overlapped with the $3\nu_Q$ of the Ge3 site. The Lorenzian and Gaussian components $1/T_2$ were observed below and above T_N, respectively. They were fitted with $M(2\tau)/M_0 \propto \exp(-2\tau/T_2)$ (Lorenzian), and $M(2\tau)/M_0 \propto \exp[-(2\tau)^2/2T_2^2]$ (Gaussian), respectively. Here, τ is the interval between two rf pulses ($\pi/2$ and π pulses) in spin–echo method.

We begin with the P-induced evolution of the antiferromagnetism in $CeNiGe_3$. The NQR spectra for the $4\nu_Q$ transition of the Ge3 site in PM state at $P = 0$, 2.0, and 2.8 GPa are indicated in the upper parts of Fig. 2(b). As T decreases below T_N, the NQR spectrum exhibits a double-peak structure due to the appearance of H_{int} associated with the AFM order. A separation between the two peaks in the NQR spectrum is related to the H_{int} that is proportional to the staggered magnetization M_Q below T_N. By extrapolating the T dependence of H_{int}, we obtain $T_N = 5.1$, 7.4, and 8.2 K and the saturated $H_{int} = 0.70$, 0.86, and 0.91 kOe at $P = 0$, 2.0, and 2.8 GPa, respectively. As observed in the phase diagram in Fig. 1, the fact that T_N increases with an application of P is corroborated by the present experiment. Since a hyperfine coupling constant A_{hf} is estimated to be ~ 0.86 kOe/μ_B at the Ge3 site, by using $M_Q \sim 0.8\mu_B$ at ambient P,[14] M_Q can be as large as $\sim 1.0\,\mu_B$ at 2.8 GPa. These results indicate that the AFM order becomes robust against increasing values of P, where SC1 occurs with a maximum T_{SC} of 0.3 K.[11]

Figure 3 shows the T dependence of $1/T_1$ at the Ge1 site at $P = 0$, 2.0, and 2.8 GPa. In the PM state, the $1/T_1$ at $P = 0$ stays almost constant above T_N, revealing that Ce 4f-derived moments behave as if they are localized. As P increases, the $1/T_1$s at $P = 2.0$ and 2.8 GPa start to decrease below $T^* \sim 14$ and 18 K, respectively, which are well above $T_N \sim 8$ K. It indicates the P-induced increase in hybridization with conduction electrons makes the 4f electrons itinerant below T^*, which resembles the case of $CeRhIn_5$.[15] These results suggest that the P-induced increase in hybridization with conduction electrons may lead to an onset of SC1. However, $T_N(P)$ and $H_{int}(P) \propto M_Q(P)$ are not expected to increase in such an itinerant regime of Ce 4f electrons.

Next, we consider the SC characteristics. As revealed by the T dependence of $1/T_1$ at $P = 2.8$ GPa, an observation of $T_1T =$ const. behavior points to the presence of the Fermi surface in the AFM state well below $T_N = 8.2$ K. Remarkably, a distinct decrease in $1/T_1T$ below $T_{SC} = 0.2$ K provides microscopic evidence of the emergence of SC1, which coexists with the antiferromagnetism. In fact, this onset of SC1 at $P = 2.8$ GPa is corroborated by the diamagnetism in ac-susceptibility χ_{ac} measured by the *in-situ* NQR coil, as shown in the inset of Fig. 3. Here, the T-derivative of χ_{ac}, $d\chi_{ac}/dT$, exhibits a peak at $T_{SC} = 0.2$ K. It should be noted that a bulk $T_{SC} = 0.2$ K is lower than $T_{SC} \sim 0.3$ K obtained by resistivity at $P = 2.9$ GPa.[11] Below $T_{SC} = 0.2$ K, $1/T_1$ shows no coherence peak, subsequently, it exhibits a power-law like T^n ($n = 2$–3) variation, and upon further cooling, it approaches a T-linear behavior. These behaviors are associated with an unconventional superconductivity with a line node in the SC gap function

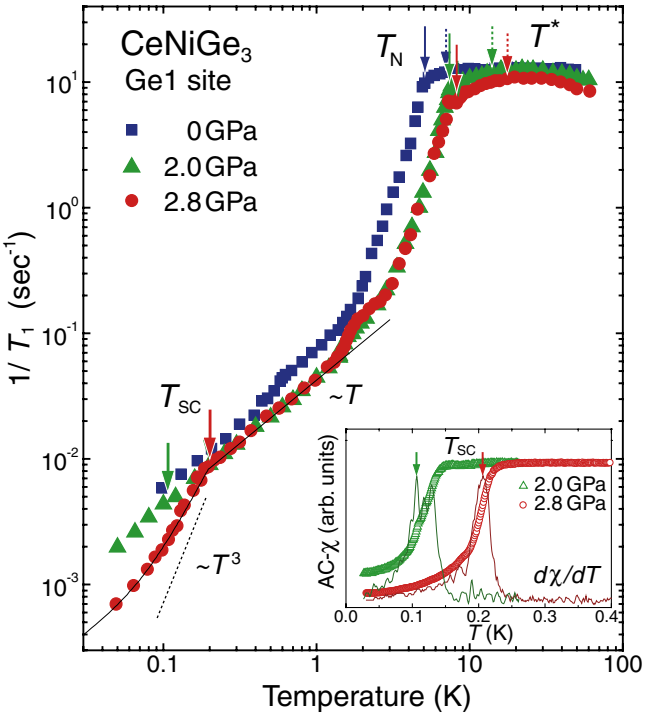

Fig. 3. (Color online) Temperature dependence of $1/T_1$ at $P = 0$, 2.0, and 2.8 GPa at the Ge1 site. At $P = 2.0$ and 2.8 GPa, SC1 emerges inside the AFM phase far from the QCP. The solid curve below $T_{SC} = 0.2$ K is obtained from a calculation based on a line node in the SC gap with $2\Delta_0/k_B T_{SC} = 4.6$ and $N_{res}/N_0 = 0.56$. The inset shows the T dependences of ac-susceptibility (open symbols) and $d\chi_{ac}/dT$ (dotted lines) at $P = 2.0$ and 2.8 GPa.

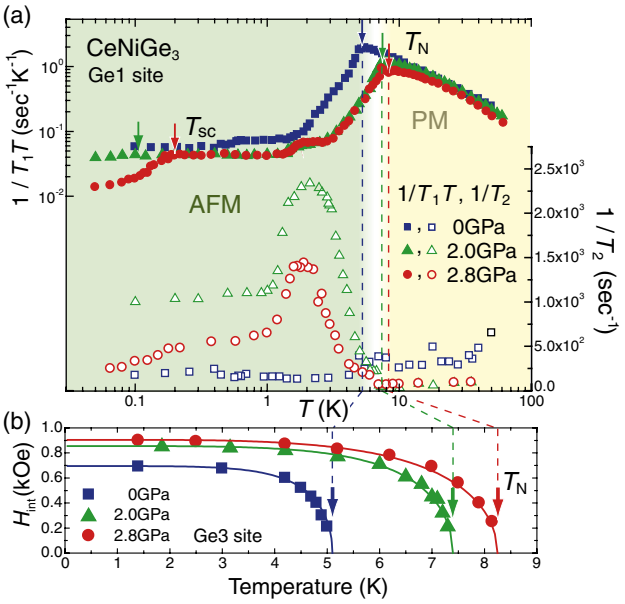

Fig. 4. (Color online) (a) Temperature dependence of $1/T_1T$ and $1/T_2$ for the Ge1 site at $P = 0$, 2.0, and 2.8 GPa. Note that $1/T_2$ exhibits a distinct peak at $T \sim 2$ K well below T_N, but far above T_{SC}; $1/T_1T$ decreases at $P = 2.0$ and 2.8 GPa. (b) Temperature dependence of $H_{int}(T)$ at $P = 0$, 2.0, and 2.8 GPa. The solid curves seen as a guide to the eye whose extrapolations to $T = 0$ and $H_{int} = 0$ give rise to $H_{int}(0) = 0.70$, 0.86, and 0.91 kOe and $T_N = 5.1$, 7.4, and 8.2 K at $P = 0$, 2.0, and 2.8 GPa, respectively.

with a finite residual density of state (N_{res}) at the Fermi level, which used to be observed in other HF SC compounds such as $CeCu_2Si_2$,[16] $CeRhIn_5$,[8,9] and $CeCoIn_5$.[17] As shown by a solid curve in Fig. 3, the line-node gap model with $\Delta(\theta) = \Delta_0 \cos\theta$ is consistent with the $1/T_1$ data below T_{SC} by assuming parameters of $2\Delta_0/k_B T_{SC} = 4.6$ and $N_{res}/N_0 = 0.56$. Here, N_0 is the density of state (DOS) at the Fermi level in the AFM state. The large fraction of $N_{res}/N_0 = 0.56$ indicates a novel SC character with a finite weight of low-lying quasiparticle excitations due to the uniformly coexisting state of SC1 and AFM states as argued in $CeRhIn_5$.[8,9] As shown in the inset of Fig. 3, the T dependences of ac-susceptibility and $d\chi_{ac}/dT$ at $P = 2.0$ GPa reveal an onset of SC at $T_{SC} \sim 0.11$ K. We cannot observe a clear decrease in $1/T_1$ below $T_{SC} \sim 0.11$ K; this suggests that a SC gap does not fully open at $P = 2.0$ GPa. A residual DOS is tentatively estimated to be as large as $N_{res}/N_0 \sim 0.95$. Evidently, some impurity effect fails to explain the P dependence of the residual DOS such as $N_{res}/N_0 = 0.95$ and 0.56 at $P = 2.0$ and 2.8 GPa, respectively.

Figure 4 shows the T dependence of the nuclear spin-spin relaxation rate $1/T_2$ at $P = 0$, 2.0, and 2.8 GPa at the Ge3 site, along with $1/T_1T$. It should be noted that $1/T_2$ can probe longitudinal low-lying magnetic excitations against the quantization axis of nuclear spin, whereas $1/T_1$ probes the transversal excitations. This is because $1/T_1$ and $1/T_2$ are generally given as $1/T_1 = A^2/2\hbar^2 \int_{-\infty}^{\infty} \cos\omega_0\tau \times \langle [S_+(\tau)S_-(0)]\rangle \, d\tau$ and $1/T_2 = 1/2T_1 + A^2/2\hbar^2 \int_{-\infty}^{\infty} \times \langle [S_z(\tau)S_z(0)]\rangle \, d\tau$, where the z axis is the quantization axis. Here, $[S_+(\tau)S_-(0)]$ and $[S_z(\tau)S_z(0)]$ correspond to the xy-plane and the z components of the spin–spin correlation functions, respectively, and A is the hyperfine coupling constant.[18] A remarkable result is that $1/T_2$ gradually increases and exhibits a prominent peak at $T \sim 2$ K in the AFM state under P, whereas $1/T_1T$ decreases suddenly at T_N and $T \sim 2$ K, as shown in Fig. 4. It should be noted that the peak in $1/T_2$ at $P = 0$ is absent, but a distinct peak in $1/T_2$ appears on applying P. It is noteworthy that there is no report on such a marked peak in $1/T_2$ below T_N in other Ce-based superconductors. Since the anomaly at $T \sim 2$ K has not been observed in specific-heat measurements under P,[19] the anomaly cannot be attributed to some phase transition, but rather due to some changes in the characteristics of magnetic fluctuations or a gradual change of AFM structure. Furthermore, it is observed that the NQR spectral shape changes on cooling below ~2 K at $P = 2.8$ GPa, suggesting a change of AFM structure. Therefore, we focus on the T-derived evolution of the NQR spectrum for the $4\nu_Q$ transition at the Ge3 site. This is because the appearance of the largest value of H_{int} at the Ge3 site enables us to sensitively detect a possible change in the AFM structure.

In the AFM state at $P = 0$ GPa, the NQR intensity between the double peaks in the spectrum can be continuously observed, which suggests a possible distribution in H_{int} relevant to the incommensurate structure of the AFM order with a propagation vector $\boldsymbol{Q} = [0, 0.409, 0.5]$ by the neutron-powder diffraction at $P = 0$.[14] At $P = 2.0$ and 2.8 GPa, however, it should be noted that as T is reduced, the NQR intensity I_0 at the center with $H_{int} = 0$ decreases, and hence, each spectral width becomes sharp, as shown in Fig. 5(a). Indeed in Fig. 5(b), I_0 markedly decreases below $T_A \sim 1.9$

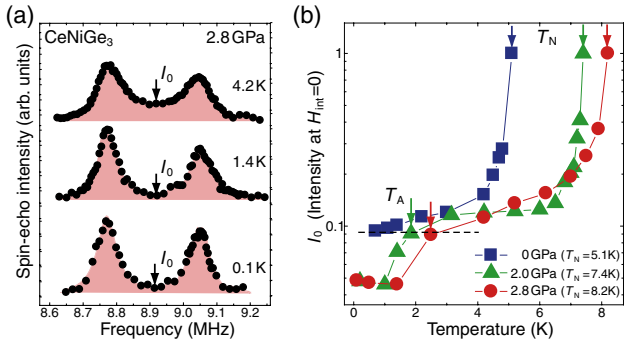

Fig. 5. (Color online) (a) The NQR spectra for the AFM state at $T = 4.2$, 1.4, and 0.1 K lower than $T_{SC} = 0.2$ K at $P = 2.8$ GPa. (b) Temperature dependence of the NQR intensity I_0 at the center with $H_{int} = 0$ at $P = 0$, 2.0, and 2.8 GPa. I_0 markedly decreases below $T_A \sim 1.9$ and 2.5 K at $P = 2.0$ and 2.8 GPa, respectively, suggesting the transition from the incommensurate spin-density-wave order into the commensurate AFM phase.

and 2.5 K at $P = 2.0$ and 2.8 GPa, respectively. This fact reveals that M_Q is no longer widely distributed at low T, suggesting the transition from the incommensurate spin-density-wave order to the commensurate AFM phase. These T_As coincide with $T \sim 2$ K around which $1/T_2$ exhibits the peak. Interestingly, as T_A and T_N increase with P, T_{SC} is enhanced as observed in Fig. 1. A commensurate AFM order should be stable, accompanying a change in the wave vector Q_b below $T_A \sim 1.9$ and 2.5 K at $P = 2.0$ and 2.8 GPa, respectively. This change in the AFM spin structure may spatially distribute the AFM spin density, causing longitudinal spin-density fluctuations on cooling. As a result, a longitudinal component of H_{int} fluctuates at the Ge1 site, which enables us to observe the peak in $1/T_2$. It is likely that the longitudinal spin-density fluctuations would be soften below T_A, and they may be a mediator of SC1 emerging in the AFM state. Notably, this longitudinal spin-density fluctuation was also indicated at the end point of the quantum first-order transition from FM2 to FM1 in the ferromagnetic superconductor UGe_2.[20,21] We suggest that the longitudinal spin-density fluctuation may be the another possible mechanism for enhancing T_{sc} in magnetic state.

In conclusion, the ^{73}Ge-NQR measurements of $CeNiGe_3$ under P have revealed that the application of P increases T_N and T_A, around which a successive transition takes place from the incommensurate spin-density-wave order to the commensurate AFM. The unconventional SC1 emerges under the background of the commensurate antiferromagnetism far from the QCP, with an increase in T_{SC} as T_N and T_A also increase. A characteristic feature of SC1 is that a large fraction of low-lying excitations remains in the quasiparticle excitation spectrum along with the uniform coexistence with antiferromagnetism. These novel phenomena in $CeNiGe_3$ have hitherto never been reported in the P–T phase diagrams among HF compounds.

Acknowledgments

We would like to thank M. Yashima, H. Kotegawa, and T. C. Kobayashi for fruitful discussions and comments. This work was supported by a Grant-in-Aid for Creative Scientific Research (15GS0213) from the Ministry of Education, Culture, Sports, Science and Technology (MEXT) and the 21st Century COE Program (G18) supported by the Japan Society for the Promotion of Science (JSPS). A.H. was financially supported by a Grant-in-Aid for Exploratory Research of MEXT (No. 17654066).

1) F. Steglich, J. Aarts, C. D. Bredl, W. Lieke, D. Meschede, W. Franz, and H. Schäfer: Phys. Rev. Lett. **43** (1979) 1892.
2) D. Jaccard, K. Behnia, and J. Sierro: Phys. Lett. A **163** (1992) 475.
3) F. M. Grosche, S. R. Julian, N. D. Mathur, and G. G. Lonzarich: Physica B **223–224** (1996) 50.
4) R. Movshovic, T. Graf, D. Mandrus, J. D. Thompson, J. L. Smith, and Z. Fisk: Phys. Rev. B **53** (1996) 8241.
5) N. D. Mathur, F. M. Grosche, S. R. Julian, I. R. Walker, D. M. Freye, R. K. W. Haselwimmer, and G. G. Lonzarich: Nature **394** (1998) 39.
6) H. Hegger, C. Petrovic, E. G. Moshopoulou, M. F. Hundley, J. L. Sarrao, Z. Fisk, and J. D. Thompson: Phys. Rev. Lett. **84** (2000) 4986.
7) T. Mito, S. Kawasaki, Y. Kawasaki, G.-q. Zheng, Y. Kitaoka, D. Aoki, Y. Haga, and Y. Ōnuki: Phys. Rev. Lett. **90** (2003) 077004.
8) M. Yashima, S. Kawasaki, H. Mukuda, Y. Kitaoka, H. Shishido, R. Settai, and Y. Ōnuki: Phys. Rev. B **76** (2007) 020509.
9) S. Kawasaki, T. Mito, Y. Kawasaki, G.-q. Zheng, Y. Kitaoka, D. Aoki, Y. Haga, and Y. Ōnuki: Phys. Rev. Lett. **91** (2003) 137001.
10) M. Nakashima, K. Tabata, A. Thamizhavel, T. C. Kobayashi, M. Hedo, Y. Uwatoko, K. Shimizu, R. Settai, and Y. Ōnuki: J. Phys.: Condens. Matter **16** (2004) L255.
11) H. Kotegawa, K. Takeda, T. Miyoshi, S. Fukushima, H. Hidaka, T. C. Kobayashi, T. Akazawa, Y. Ohishi, M. Nakashima, A. Thamizhavel, R. Settai, and Y. Ōnuki: J. Phys. Soc. Jpn. **75** (2006) 044713.
12) A. Harada, S. Kawasaki, H. Mukuda, Y. Kitaoka, A. Thamizhavel, Y. Okuda, R. Settai, Y. Ōnuki, K. M. Itoh, E. E. Haller, and H. Harima: J. Magn. Magn. Mater. **310** (2007) 614.
13) A. S. Kirichenko, A. V. Kornilov, and V. M. Pudalov: Instrum. Exp. Tech. **48** (2005) 813.
14) L. Durivault, F. Bourée, B. Chevalier, G. André, F. Weill, J. Etourneau, P. Martinez-Samper, J. G. Rodrigo, H. Suderow, and S. Vieira: J. Phys.: Condens. Matter **15** (2003) 77.
15) S. Kawasaki, T. Mito, G.-q. Zheng, C. Thessieu, Y. Kawasaki, K. Ishida, Y. Kitaoka, T. Muramatsu, T. C. Kobayashi, D. Aoki, S. Araki, Y. Haga, R. Settai, and Y. Ōnuki: Phys. Rev. B **65** (2001) 020504.
16) Y. Kitaoka, K. Ueda, T. Kohara, K. Asayama, Y. Ōnuki, and T. Komatsubara: J. Magn. Magn. Mater. **52** (1985) 341.
17) M. Yashima, S. Kawasaki, Y. Kawasaki, G.-q. Zheng, Y. Kitaoka, H. Shishido, R. Settai, Y. Haga, and Y. Ōnuki: J. Phys. Soc. Jpn. **73** (2004) 2073.
18) C. P. Slichter: *Principles of Magnetic Resonance* (Springer, Heidelberg, 1998).
19) N. Tateiwa, Y. Haga, T. D. Matsuda, S. Ikeda, M. Nakashima, A. Thamizhavel, R. Settai, and Y. Ōnuki: *Proc. 5th Int. Symp. ASR-WYP-2005: Advances in the Physics and Chemistry of Actinide Compounds*, J. Phys. Soc. Jpn. **75** (2006) Suppl., p. 174.
20) A. D. Huxley, S. Raymond, and E. Ressouche: Phys. Rev. Lett. **91** (2003) 207201.
21) A. Harada, S. Kawasaki, H. Mukuda, Y. Kitaoka, Y. Haga, E. Yamamoto, Y. Ōnuki, K. M. Itoh, E. E. Haller, and H. Harima: Phys. Rev. B **75** (2007) 140502.